Available online at www.sciencedirect.com
ScienceDirect
Trans. Nonferrous Met. Soc. China 32(2022) 162−174
Transactions of Nonferrous Metals Society of China
www.tnmsc.cn

Quantitative characterization of lamellar α precipitation behavior of IMI834 Ti-alloy in isothermal and non-isothermal heat treatments

Xue-yan LIU[1,2], Hong-wei LI[1,2], Mei ZHAN[1,2], Hong-rui ZHANG[1,2]

1. State Key Laboratory of Solidification Processing, School of Materials Science and Engineering, Northwestern Polytechnical University, Xi'an 710072, China;
2. Shaanxi Key Laboratory of High-Performance Precision Forming Technology and Equipment, Northwestern Polytechnical University, Xi'an 710072, China

Received 7 January 2021; accepted 10 July 2021

Abstract: To reveal the affecting mechanism of cooling rate on lamellar α precipitation, the precipitation behaviors of lamellar α phase in IMI834 titanium alloy during isothermal and non-isothermal heat treatments were quantitatively characterized using experimental analysis. Critical precipitation temperatures at various cooling rates were obtained using thermal dilatation testing. Using metallographic microscopy, electron microprobe analysis, and data fitting methods, the quantitative evolution models of average width, volume fraction, and solute concentration in the α and β phases were built for different temperatures or cooling rates. A comparison between the two precipitation behaviors showed that the average width and volume fraction of lamellar α phase under non-isothermal conditions were smaller than those under isothermal conditions. With increasing cooling rate, the average width and volume fraction were decreased significantly, and the critical precipitation temperatures were reduced. This phenomenon is mainly attributed to the decreased diffusion velocity of solutes Al, Mo, and Nb with increasing cooling rate.

Key words: heat treatment; lamellar α phase; precipitation; morphology evolution; critical precipitation temperature; volume fraction model; solute concentration evolution model

1 Introduction

Near-α IMI834 titanium alloy, which exhibits high ultimate tensile strength at room temperature (i.e., 1030 MPa), high operating temperatures (i.e., 600 °C), and good combinations of creep and fatigue resistance at elevated temperatures, has been widely used in various aeroengine rotor (discs, shafts, and blades) and stator (rings and blades) components [1−4]. The typical microstructures of titanium alloys consist of a lamellar α phase, an equiaxial α phase, and a transformed β matrix with multifarious proportions, morphologies, and distributions [5]. Since the high-density boundaries of the lamellar structure shorten the effective slip length of dislocations and cause tortuosity of the crack path, the lamellar α phase determines the fracture toughness, fatigue crack propagation resistance, and creep properties of the alloy [6−9]. Therefore, understanding the lamellar α evolution rules and mechanisms of IMI834 titanium alloy is vital for controlling microstructure and tailoring properties of this alloy.

In general, heat treatment, comprising heat preservation in the β phase and subsequent cooling, is applied to producing α lamellar (i.e., colony or Widmanstatten pattern) microstructure [5]. The microstructural features of lamellar α, such as the morphology, volume fraction, and size, are a function of soak temperature in the α+β field and cooling rate [10−13]. Thus, accurately characterizing

Corresponding author: Hong-wei LI, Tel: +86-29-88460212, E-mail: lihongwei@nwpu.edu.cn
DOI: 10.1016/S1003-6326(21)65785-0

the quantitative evolution of lamellar α features under various heat treatment conditions is pivotal and necessary for revealing the lamellar α evolution rules and mechanisms.

At present, there are two main methods for the quantitative characterization of lamellar α feature evolution under heat treatment conditions. One method is to make a numerical prediction based on solute diffusion theory [14−16], and the other method requires the establishment of simple mathematical relationships by heat treatment experiments and quantitative metallography analysis [17−19]. SEMIATIN et al [10,20] developed a growth model of equiaxed and lamellar α that revealed the effects of solution temperature of the α+β phase and cooling rate on the volume fraction evolution during heat treatment of Ti−6242Si and Ti−6Al−4V titanium alloys. However, a big gap exists between simulation and experiments. This discrepancy suggested that the effect of the temperature paths should be considered. Simulation results obtained by MENG et al [21] also proved that the effect of the temperature paths was significant. Additionally, MENG et al [21] developed a new growth model of equiaxed α phase by considering the effect of temperature paths based on the model proposed by SEMIATIN et al [10]. The simulated volume fraction of equiaxed α showed little difference from the experimental data. From a macroscopic perspective, the improved model by MENG et al [21] has become a significant predictor of the average volume fraction and precipitation kinetics for equiaxed α phase. However, this model was still unable to predict complex morphological lamellar structure evolution at the microscopic level and cannot eliminate the volume fraction deviation caused by the lamellar morphology. Although SONG et al [22] combined the cellular automata method and growth model of lamellar α phase to try to simulate the morphological evolution of lamellar α phase, the simulated results showed a great discrepancy with experiments in terms of volume fraction and lamellae width because the temperature history was not considered. In summary, the inner formation mechanism of lamellar α phase with different temperature histories was still unclear. Using the latter quantitative characterization method, SENKOV et al [23] observed that the average width of lamellar α phase decreased from 9 to 7 μm with an increase in the cooling rate from 20 to 490 K/min during heat treatment of Ti−6Al−4V titanium alloys in the α+β phase. Furthermore, the main solutes Al and V, in α and β phases exhibited large changes. BEHERA et al [24] reported that by increasing the cooling rate from 20 to 90 K/min, the beginning and ending temperatures of the lamellar α precipitation of Ti−5Ta−1.8Nb alloy decreased from 854 to 826 °C and from 749 to 705 °C, respectively. Additionally, the average width of lamellar α phase decreased from 6 to 2.5 μm, and diffusion of the main solutes Ta and Nb slowed in the β phase. The slow diffusion of the main solutes Ta and Nb further resulted in a change in the precipitation mode from diffusion to non-diffusion. The above studies suggested that the solute concentration evolution, temperature, and cooling rate controlled the lamellar α phase precipitation features. For different alloys, different dominant solutes give rise to different evolution rules for lamellar α phase precipitation. For the IMI834 alloy, the evolution rules of lamellar α phase precipitation features controlled by dominant solutes during heat treatment remain unknown.

Accordingly, in order to reveal the quantitative effect mechanism of cooling rate on lamellar α phase evolution for IMI834 titanium alloy, the precipitation behaviors of lamellar α phase during isothermal and non-isothermal heat treatments were both quantitatively acquired. Under isothermal conditions, the evolutions of the average width, volume fraction, and solute concentration in α and β phases as functions of temperature were determined quantitatively. Under non-isothermal conditions, the critical precipitation temperatures, volume fraction, and solute concentration evolution models in α and β phases as functions of temperature and cooling rate were established. Furthermore, a contrastive analysis of lamellar α phase precipitation behaviors under these two conditions was also carried out.

2 Experimental

The material used in this work was IMI834 titanium alloy. The measured chemical composition was 6.03 wt.% Al, 4.10 wt.% Sn, 3.71 wt.% Zr, 0.52 wt.% Mo, 0.65 wt.% Nb, and the balance Ti. The β-transus temperature determined via a series of heat treatment experiments and metallographic examinations was 1058 °C. The as-received room-

temperature microstructure of the alloy that is shown in Fig. 1 contained 65.12 wt.% primary equiaxed α phase with an average diameter of 21.21 μm.

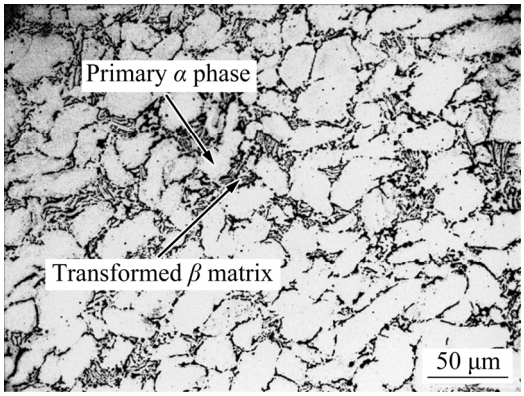

Fig. 1 Initial microstructure of IMI834 titanium alloy

The purpose of the experiments was to investigate the quantitative evolution rules of lamellar α phase features such as average width, volume fraction, solute concentration in the α and β phases, and critical precipitation temperatures as functions of temperature and cooling rate in isothermal and non-isothermal transformation processes. Cylindrical Specimens I (d10 mm × 15 mm) and II (d3 mm × 10 mm) were machined from the as-received bar. Cylindrical Specimen I was used for microstructure observations and quantitative analyses in terms of average width, volume fraction, and solute concentration in α and β phases, whereas cylindrical Specimen II was used to determine the critical precipitation temperatures under non-isothermal conditions. The details of the experimental scheme are shown in Table 1.

Under isothermal conditions, a heat treatment of (1120 °C, 10 min, air cooling (AC)) was applied to Specimen I according to the research conducted by CHANG et al [25]. The treated specimens were then heated to the corresponding temperature ranging from 840 to 1020 °C at 30 °C intervals and held for 2 h. Subsequently, water quenching (WQ) was performed.

Under non-isothermal conditions, Specimen I was heated to 1120 °C, held for 10 min, and then cooled at constant rates of 30, 72, and 150 °C/min. Finally, these specimens were water-quenched after reaching prescribed temperatures of 1020, 960, 900, and 840 °C. To determine the beginning and ending temperatures of lamellar α phase precipitation at various cooling rates, the dilatometer measurement was performed on Specimen II using a Gleeble 3800 thermo-mechanical simulator. The specific

Table 1 Heat treatment experimental schemes

No.	Isothermal transformation	Non-isothermal transformation	
	Specimen I	Specimen I	Specimen II
1	(1120 °C, 10 min, AC) + (1020 °C, 2 h, WQ)	(1120 °C, 10 min) → (1020 °C (30 °C/min), WQ)	(1120 °C, 10 min) → RT (12 °C/min)
2	(1120 °C, 10 min, AC) + (990 °C, 2 h, WQ)	(1120 °C, 10 min) → (960 °C (30 °C/min), WQ)	(1120 °C, 10 min) → RT (30 °C/min)
3	(1120 °C, 10 min, AC) + (960 °C, 2 h, WQ)	(1120 °C, 10 min) → (900 °C (30 °C/min), WQ)	(1120 °C, 10 min) → RT (48 °C/min)
4	(1120 °C, 10 min, AC) + (930 °C, 2 h, WQ)	(1120 °C, 10 min) → (840 °C (30 °C/min), WQ)	(1120 °C, 10 min) → RT (72 °C/min)
5	(1120 °C, 10 min, AC) + (900 °C, 2 h, WQ)	(1120 °C, 10 min) → (1020 °C (72 °C/min), WQ)	(1120 °C, 10 min) → RT (108 °C/min)
6	(1120 °C, 10 min, AC) + (870 °C, 2 h, WQ)	(1120 °C, 10 min) → (960 °C (72 °C/min), WQ)	(1120 °C, 10 min) → RT (150 °C/min)
7	(1120 °C, 10 min, AC) + (840 °C, 2 h, WQ)	(1120 °C, 10 min) → (900 °C (72 °C/min), WQ)	(1120 °C, 10 min) → RT (240 °C/min)
8		(1120 °C, 10 min) → (840 °C (72 °C/min), WQ)	(1120 °C, 10 min) → RT (360 °C/min)
9		(1120 °C, 10 min) → (1020 °C (150 °C/min), WQ)	
10		(1120 °C, 10 min) → (960 °C (150 °C/min), WQ)	
11		(1120 °C, 10 min) → (900 °C (150 °C/min), WQ)	
12		(1120 °C, 10 min) → (840 °C (150 °C/min), WQ)	

AC: Air cooling; WQ: Water quenching; RT: Room temperature

scheme is as follows: Specimen II was heated to 1120 °C at a rate of 10 °C/s and held for 10 min. The samples were then cooled at rates of 12, 30, 48, 72, 108, 150, 240, and 360 °C/min to room temperature (RT).

Metallographic preparation was carried out by sectioning the sample perpendicular to the axis in the middle of the axis, mechanical grinding, polishing, and etching with a solution of 3 vol.% HF, 10 vol.% HNO_3, and 87 vol.% H_2O. Microstructure observations were performed using an OLYMPUS PMG3 metallographic microscope. Image-Pro Plus 6.0 image analysis software was employed for quantitative analyses of the volume fraction and average width of lamellar α phase. The main solute concentration of α phase after heat treatment was determined by electron microprobe analysis in JEOL EDS System. To ensure the reliability of the experimental results, three positions were examined under each condition to determine the average solute concentration.

3 Results and discussion

3.1 Morphological evolution of lamellar α phase

The microstructures of IMI834 titanium alloy at different temperatures after isothermal and non-isothermal heat treatments are shown in Figs. 2 and 3, respectively. In these figures, the dark gray or black lamellar structure in the form of a colony was lamellar α phase, and the light gray region was the β matrix. To recognize fine lamellar α under non-isothermal conditions, the image magnification was increased (for example, Fig. 3), and the acicular and intersecting structures randomly distributed in the β matrix were martensite.

Under isothermal conditions in Fig. 2, as the transformation temperature was reduced, the volume fraction of lamellar α phase increased rapidly, the average width of lamellar α phase decreased, the length increased quickly, and the amount of cluster also increased. Under continuous cooling, as shown in Fig. 3, the average width was smaller than that of lamellar α phase under isothermal conditions. At a fixed cooling rate, the volume fraction and average width of lamellar α phase increased slowly, whereas the length increased quickly with decreasing temperature. At the same temperature, the volume fraction and average width of lamellar α phase decreased, and the morphology of α phase gradually changed from lamellar to acicular with increasing cooling rate.

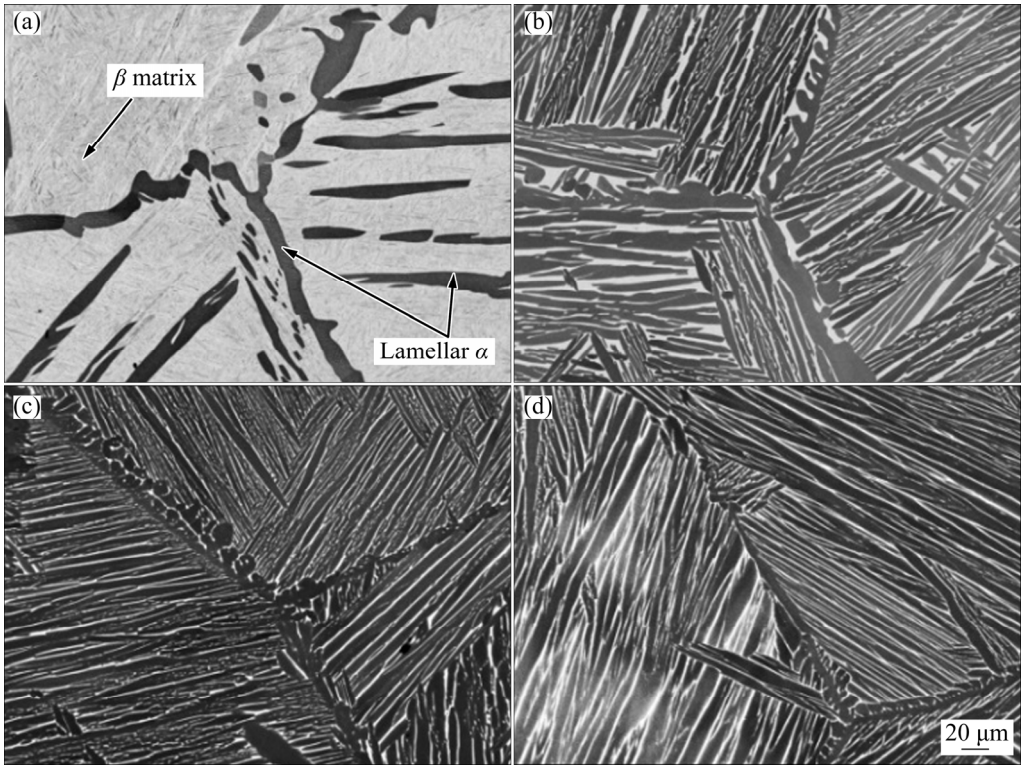

Fig. 2 Microstructures of IMI834 titanium alloy after isothermal phase transformation at various temperatures: (a) 1020 °C; (b) 960 °C; (c) 900 °C; (d) 840 °C

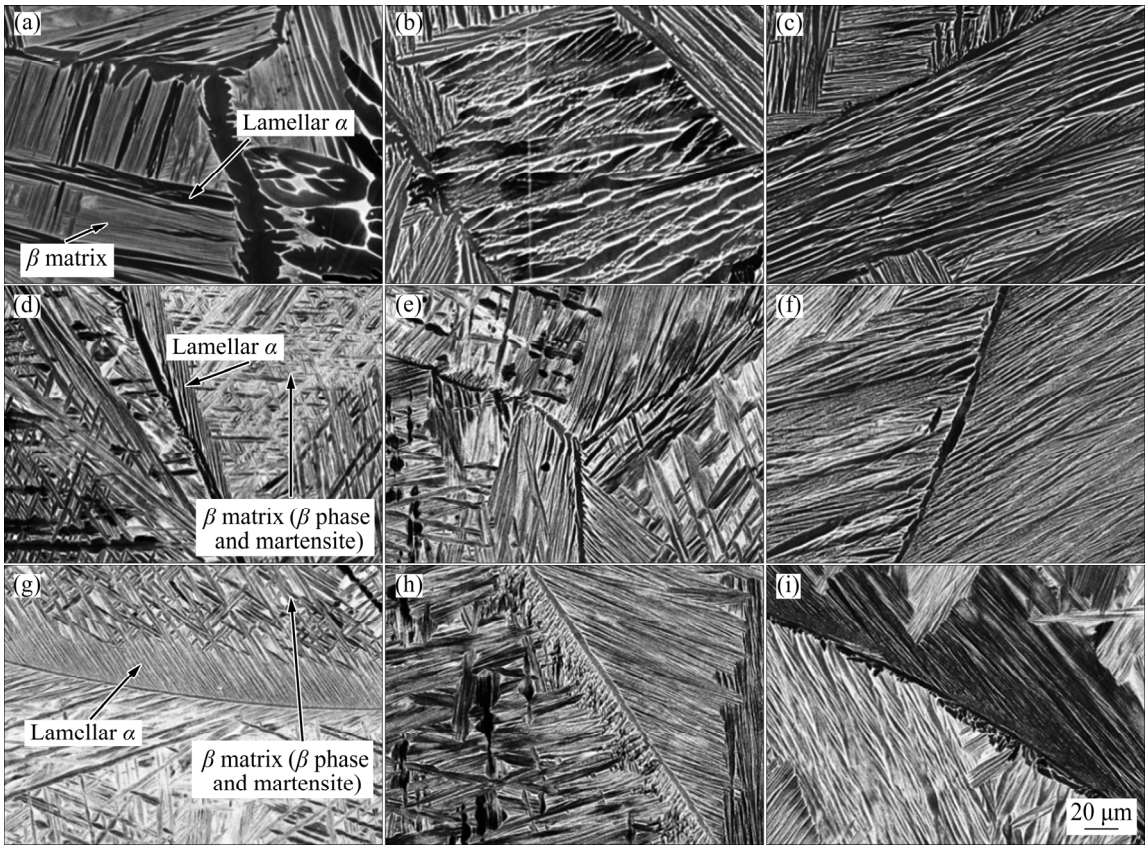

Fig. 3 Microstructures of IMI834 titanium alloy during cooling from 1120 °C to different temperatures at various cooling rates (non-isothermal heat treatments): (a) 1020 °C, 30 °C/min; (b) 900 °C, 30 °C /min; (c) 840 °C, 30 °C/min; (d) 1020 °C, 72 °C/min; (e) 900 °C, 72 °C/min; (f) 840 °C, 72 °C/min; (g) 1020 °C, 150 °C/min; (h) 900 °C, 150 °C/min; (i) 840 °C, 150 °C/min

3.2 Average width evolution of lamellar *α* phase

In Section 3.1, the average width evolution rules of lamellar *α* phase were qualitatively described in terms of the microstructure morphology under isothermal and non-isothermal conditions. This section will provide insight into the quantitative effects of temperature and cooling rate on the average width, as shown in Fig. 4.

Under isothermal conditions, the average width of lamellar *α* phase ranged from 5 to 10 μm in the temperature range from 840 to 1020 °C. The average width of lamellar *α* phase decreased by approximately 1 μm when the isothermal transformation temperature lowered by 60 °C. During continuous cooling, when the cooling rate was greater than or equal to 30 °C/min, the average width of lamellar *α* phase was less than 6.5 μm. With an increase in the cooling rate from 30 to 150 °C/min, the average width of lamellar *α* phase decreased by approximately 2 μm. Additionally, the average width of lamellar *α* phase increased by 2−3 μm when the temperature lowered from 1020 to 840 °C. The comparison between Fig. 4(a) and Fig. 4(b) showed that the average width of lamellar *α* phase under isothermal conditions was greater than that under non-isothermal conditions.

3.3 Volume fraction evolution of lamellar *α* phase

3.3.1 Under isothermal conditions

To evaluate the direction and degree of phase composition deviation of the alloy from equilibrium under non-equilibrium conditions (applying external forces such as rapid cooling or deformation), the equilibrium volume fraction is usually used as a reference standard. The equilibrium volume fraction of lamellar *α* phase as a function of temperature for IMI834 titanium alloy is shown in Fig. 5 to further investigate the influence of the cooling rate on the alloy composition.

The quantitative relationship between the equilibrium volume fraction (f_{eq}) and temperature

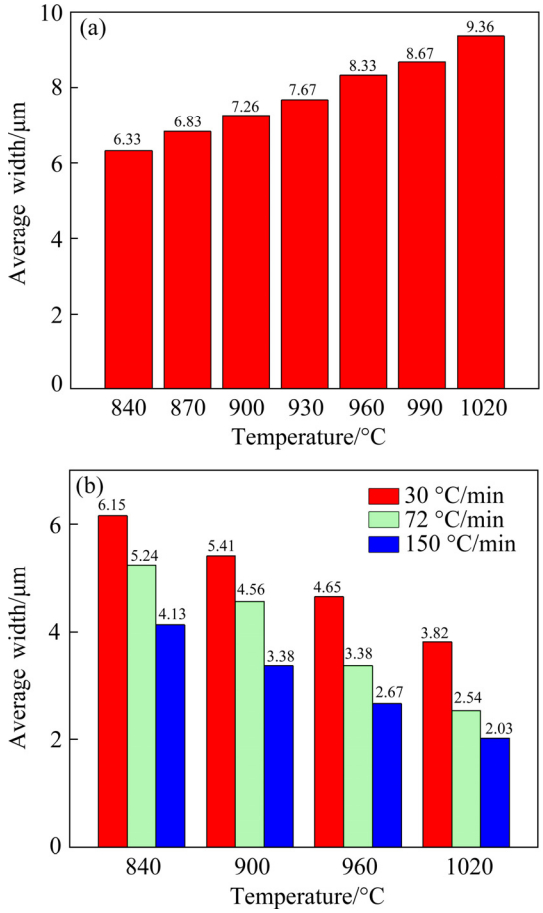

Fig. 4 Average width of lamellar α phase at different temperatures for IMI834 titanium alloy: (a) Isothermal phase transformation; (b) Continuous cooling at various cooling rates

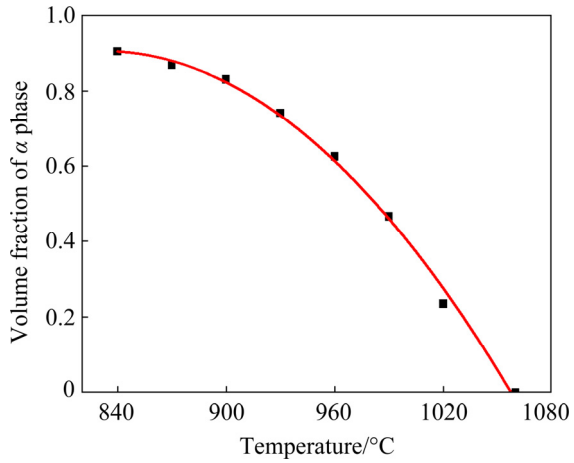

Fig. 5 Equilibrium volume fraction of lamellar α phase at different temperatures for IMI834 titanium alloy

$T(K)$ can be expressed as follows [26]:

$$f_{eq}=f_0\{1-\exp[-f_1(1331-T(K))]\} \quad (1)$$

where f_0 and f_1 are material constants. Fitting this equation to the experimental results determined that f_0 and f_1 were equal to 0.93 and 0.0109, respectively.

3.3.2 Under non-isothermal conditions

During continuous cooling, lamellar α phase precipitation occurs within a certain temperature range. A faster cooling rate usually lowers the beginning and ending temperatures of lamellar α phase precipitation, and thus significantly changes the precipitation behavior of lamellar α phase. This behavior complicates the solute concentration evolution in α and β phases and the average width and volume fraction evolutions of lamellar α phase as functions of temperature and time. Therefore, the continuous cooling transformation diagram for IMI834 titanium alloy needs to be acquired first. Then, the volume fraction of lamellar α phase at different temperatures in the phase transformation temperature range needs to be measured for various cooling rates. The above two results are finally combined to establish the volume fraction evolution rule of lamellar α phase with temperature, cooling rate, or time.

3.3.2.1 Critical precipitation temperature

The dilatometric curves along the radial direction were recorded during continuous cooling at different rates for IMI834 titanium alloy, as shown in Fig. 6.

The beginning and ending temperatures $T_{beginning}$ and T_{ending} of lamellar α phase precipitation were determined using the tangent method [27]. Based on Fig. 6, the fitting curves of the two critical temperatures and cooling rates are provided in Fig. 7.

As the cooling rate increased, the decrease in the beginning temperature was approximately linear, and the ending temperature also decreased. Furthermore, the rate of decrease for the ending temperature also decreased until the rate was approximately zero. The critical temperatures for the IMI834 alloy at various cooling rates had a similar evolution tendency to that of TA15 alloy [15].

The quantitative relations between the two critical temperatures of lamellar α phase precipitation and cooling rate can be presented as follows:

$$T_{beginning}=1049.09194-0.16739v \quad (2)$$

$$T_{ending}=817.01647-0.30999v+5.04839\times10^{-4}v^2 \quad (3)$$

where v denotes the cooling rate. The degree of

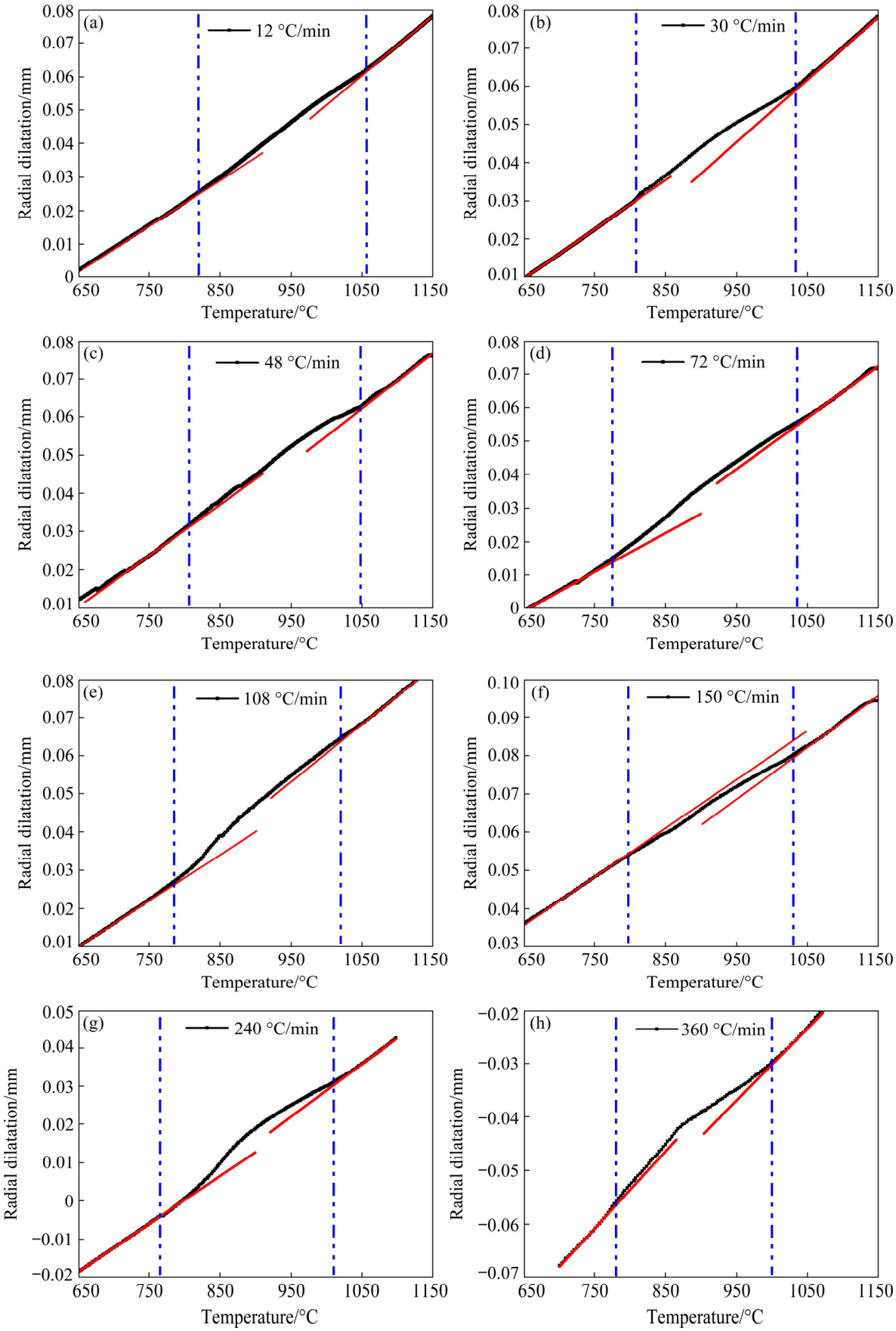

Fig. 6 Dilatometric curves along radial direction during cooling at different rates (black line) (The red line is tangent to the black line. The pointcuts correspond to the beginning or ending transformation temperatures)

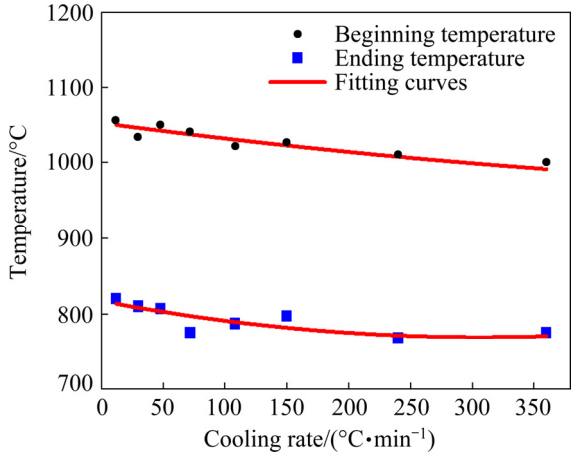

Fig. 7 Beginning and ending phase transformation temperatures as function of continuous cooling rate based on Fig. 6

undercooling can be obtained by calculating the difference in the beginning temperature from the β-transus temperature.

3.3.2.2 Modeling of volume fraction evolution and model validation

Combining with the volume fraction and the critical precipitation temperatures of lamellar α phase measured in the experiment, the fitting curves for volume fraction as a function of temperature at different cooling rates were acquired in the form of an "S"-type curve, as shown in Fig. 8.

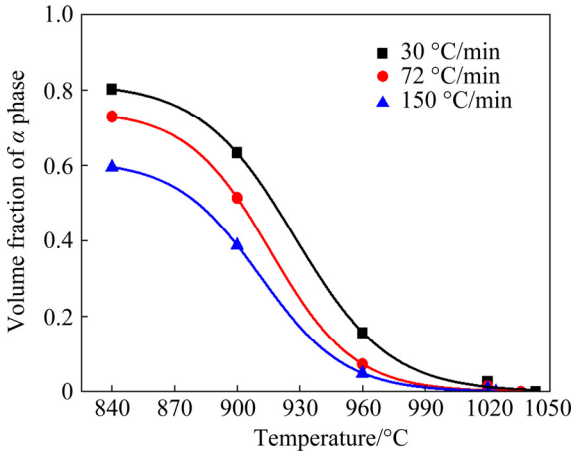

Fig. 8 Volume fraction evolution of lamellar α phase during continuous cooling at various cooling rates for IMI834 titanium alloy

The equation to fit the data in Fig. 8 can be written as follows:

$$f=A_1+\frac{A_2-A_1}{1+10^{[\lg T_0-T(K)]p}} \quad (4)$$

where f represents volume fraction, parameters A_1, A_2, lg T_0, and p are the functions of cooling rate, and $T(K)$ is temperature.

By adopting the curve fitting method, the effect of the cooling rate on parameters A_1, A_2, lg T_0, and p was determined, as shown in Fig. 9.

The parameters A_1, A_2, lg T_0, and p as the functions of cooling rate are expressed as follows:

$$A_1=(105200-1064.1v+3.46306v^2)\times10^{-7} \quad (5)$$

$$A_2=0.85977-0.00164v \quad (6)$$

$$\lg T_0=1183.30651+55.10335\exp(-0.03124v) \quad (7)$$

$$p=-0.0217-0.0017\exp(-0.01554v) \quad (8)$$

To verify the prediction accuracy of the volume fraction evolution model of lamellar α phase as the functions of temperature and cooling rate, the volume fractions of lamellar α phase at various temperatures and a cooling rate of 10 °C/min were predicted by the model. The volume fractions at 840, 900, 960, and 1020 °C and a cooling rate of 10 °C/min were measured through experiments. Additionally, the model predicted and initially measured volume fractions were compared at cooling rates of 30, 72, and 150 °C/min. As shown in Fig. 10, the errors showed that the established volume fraction evolution model was reliable and accurate.

In Figs. 8 and 10, the volume fraction of lamellar α phase increased slowly at the initial and final stages of the cooling process, while it increased quickly during the intermediate stage. The decrease in the volume fraction increased with increasing cooling rate in the intermediate and final stages of continuous cooling. Under isothermal conditions (Fig. 5), the volume fraction of lamellar α phase increased quickly in the initial and intermediate stages. Compared with the volume fraction of lamellar α phase under isothermal conditions, the volume fraction decreased by 20%−30% when the cooling rate increased from 30 to 150 °C/min.

3.4 Solute concentration evolution in α and β phases

The precipitation process of lamellar α phase relies on the diffusion of the main solutes in grains and at interfaces and the migration of interfaces. The change in the precipitation behavior of lamellar α phase under different conditions is essentially

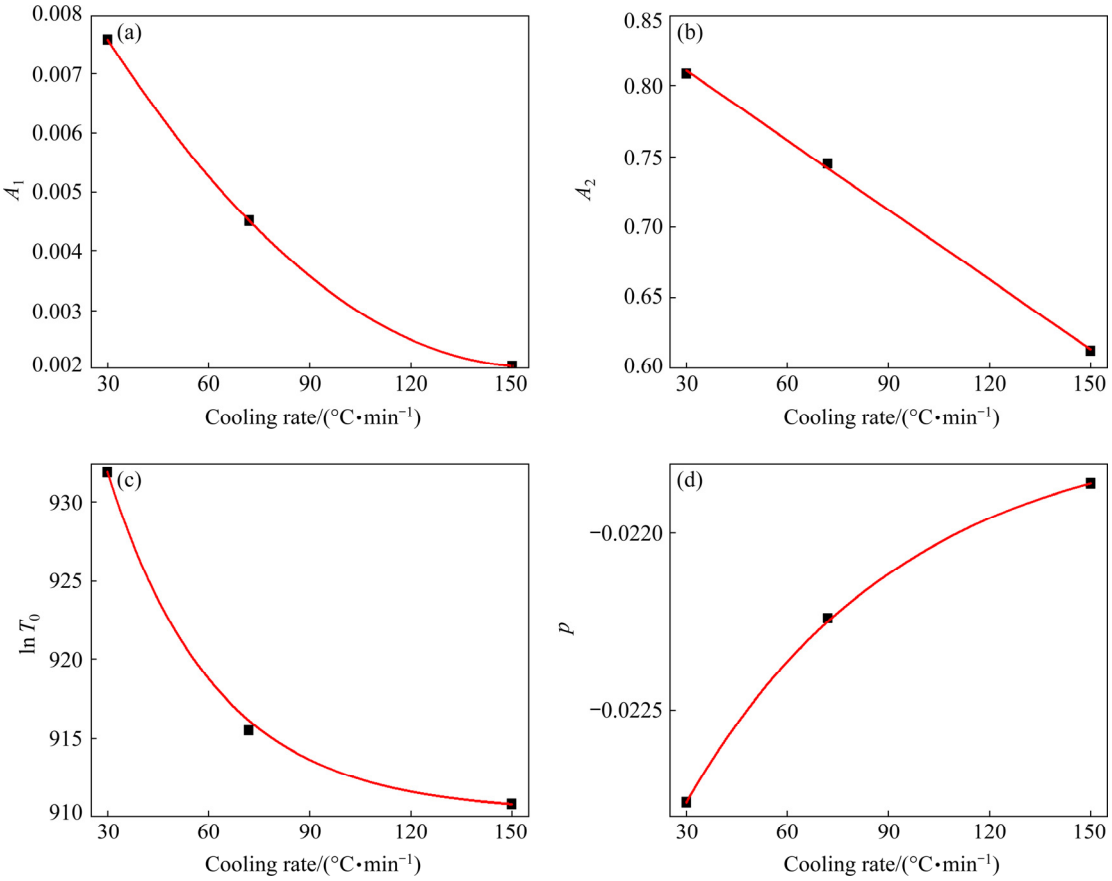

Fig. 9 Effect of cooling rate on fitting parameters A_1 (a), A_2 (b), lg T_0 (c), and p (d)

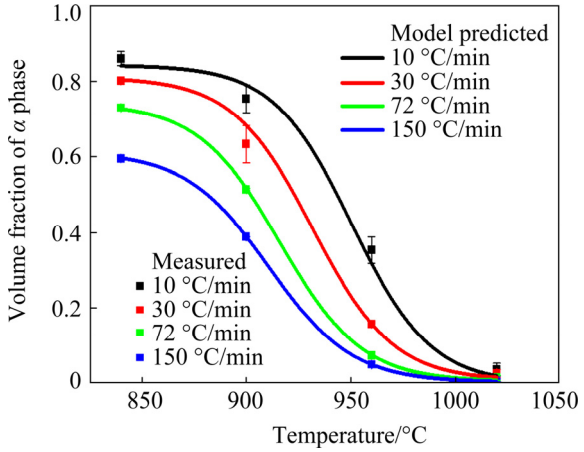

Fig. 10 Comparison of predicted and measured volume fractions of lamellar α phase during continuous cooling of IMI834 titanium alloy at different cooling rates

caused by changing the solute redistribution rules. Therefore, the concentration evolution of the main solutes in α and β phases was investigated as the functions of temperature and cooling rate. This investigation was useful for revealing the effects of temperature and cooling rate on the precipitation behavior of lamellar α phase and uncovering the internal mechanism.

3.4.1 Under isothermal conditions

The equilibrium concentrations of the main solutes Al, Mo, and Nb in α and β phases at different temperatures are shown in Fig. 11, where other solutes are independent of temperature.

In Fig. 11, the solute contents in the α phase exhibited small linear changes as the function of temperature with the slopes of the fitting curves close to zero, whereas the solute contents in the β matrix changed significantly. This figure suggests that the precipitation process of lamellar α phase is essentially Al, Mo, and Nb diffusion through the β matrix. In other words, Al is absorbed into the parent β phase, whereas Mo and Nb exit the parent β phase, which assists the parent β phase to be α phase. Owing to the weak diffusivity of Mo [10], the change in the Mo concentration in the β phase was greater than those of Al and Nb, so Mo diffusion will indeed control the growth of lamellar α phase.

3.4.2 Under non-isothermal conditions

To preserve the microstructure state, such as morphology, composition, and solute distribution at high temperatures, the specimens were quenched

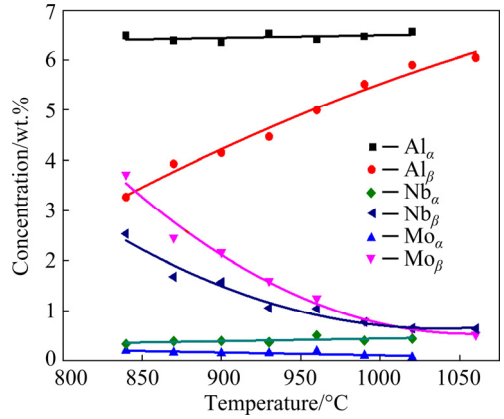

Fig. 11 Equilibrium concentrations of Al, Mo, and Nb in α and β phases as function of temperature for IMI834 titanium alloy

after continuous cooling. A mount of martensite was present in the β matrix. As the cooling rate increased, lamellar α phase became finer so that its morphology gradually approached that of martensite, and the inhomogeneity of the solute distribution in the β matrix (consisting of vast amounts of α martensite and extremely little residual β phase) decreased according to images observed from an electron probe. This phenomenon made distinguishing these three phases difficult. Therefore, the solute concentration in the β matrix was also tough to measure. The concentration evolution of the main solutes was measured only in the α phase. The solute concentration in the β phase was substituted by the solute concentration in the β matrix.

The concentrations of Al, Mo, and Nb in the α and β phases at different temperatures and various cooling rates are shown in Fig. 12.

The concentrations (X) of Al, Mo, and Nb in α phase exhibited approximately linear functions of temperature at various cooling rates in Figs. 12(a, c, e), which can be described as follows:

$$X^{\alpha}=X_0+k[T(K)-273] \quad (9)$$

where X_0 and k are the functions of the cooling rate.

For the solute Al in α phase, the parameters X_0 and k were fitted as follows:

$$X_0=6.14983+5.82915\exp(-0.0295v) \quad (10)$$

$$k=10^{-3}[-0.11135-6.22\exp(-0.0319v)] \quad (11)$$

For the solute Mo in the α phase, the parameters X_0 and k were fitted as follows:

$$X_0=10^{-5}(47974+266v-1.45215v^2) \quad (12)$$

$$k=10^{-9}(-470385+1622v-3.65032v^2) \quad (13)$$

For the solute Nb in the α phase, the parameters X_0 and k were fitted as follows:

$$X_0=10^{-5}(-14810+805v-2.43223v^2) \quad (14)$$

$$k=10^{-10}(5579766-48621v+87.6333v^2) \quad (15)$$

The concentration evolutions of the main solutes Al, Mo, and Nb in the β matrix were obtained by calculating the solute equilibrium equation based on the established volume fraction model of lamellar α phase and the solute concentration evolution model in the α phase, as shown in Figs. 12(b, d, f). The results for non-isothermal conditions in Fig. 12 proved that Mo diffusion indeed controlled the growth of lamellar α phase. As the cooling rate increased, diffusion of the solutes Al, Mo, and Nb in α and β phases gradually slowed down according to the decreased slopes in Figs. 12(a, c, e), and the variation in solute concentration decreased rapidly at the same temperatures in Figs. 12(b, d, f). During continuous cooling, the amounts of variability in the solute concentrations in α and β phases, from the initial stage to the final stage of lamellar α phase precipitation, were smaller than those under isothermal conditions.

3.5 Effect of cooling rate on lamellar α phase precipitation

Lamellar α phase precipitation is mainly composed of nucleation, growth, and impingement. The morphology and volume fraction of lamellar α during continuous cooling depend on the effect of the cooling rate on nucleation, growth, and impingement. The results in Section 3.4 imply that an increase in the cooling rate did not provide enough time for the solutes Mo and Nb to exit the parent β phase and for the solute Al to be absorbed into the parent β phase, which resulted in a decrease in the solute diffusion velocity (see Fig. 12). During cooling, if the temperature is reduced below the equilibrium transformation critical point, the supersaturation degree of the solutes will increase [28]. When the decrease in the diffusion velocity and the increase in the supersaturation degrees of solutes both appear, the degree of supercooling increases, and the beginning and ending temperatures of lamellar α phase precipitation decrease. At the same time, the nucleation energy required for the critical nucleus

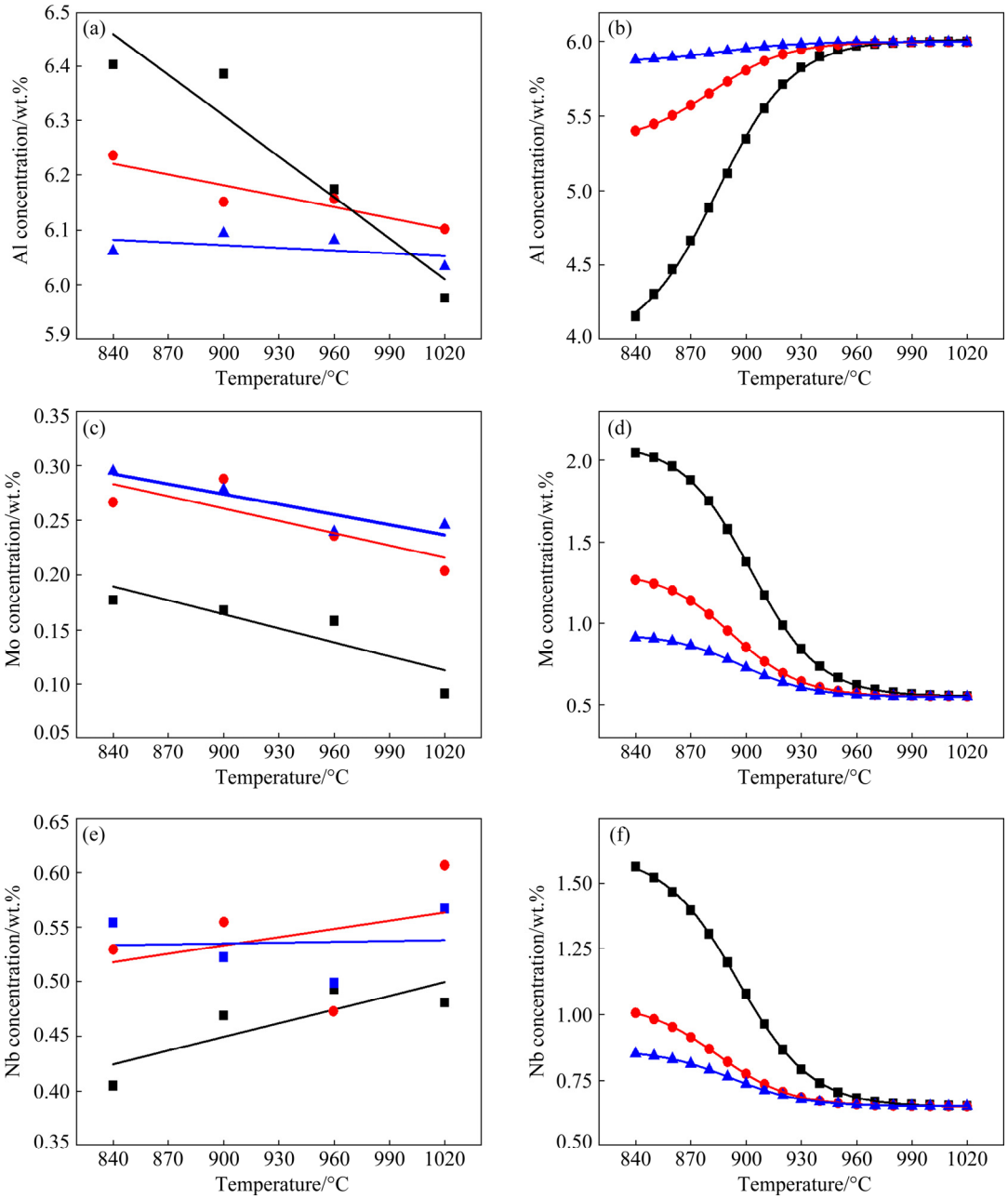

Fig. 12 Concentrations of Al, Mo, and Nb in α (a, c, e) and β (b, d, f) phases as function of temperature at various cooling rates

reduces, and the nucleation rate also increases [29]. When the cooling rate is sufficiently high and the temperature is sufficiently low, the nucleation rate is very high. An extremely large nucleation rate limits the growth space of the lamellar α phase [28]. This limited space is the essential reason that the lamellae are slender with a higher cooling rate. With a decrease in the diffusion velocity of the solutes, the growth velocity of lamellar α phase decreases. Therefore, the volume fraction of lamellar α phase under non-isothermal conditions is smaller than under isothermal conditions, and the deviation of the volume fraction from equilibrium increases with increasing cooling rate in the intermediate and final stages of lamellar α phase precipitation.

4 Conclusions

(1) The average width and volume fraction of lamellar α phase were smaller under non-isothermal conditions than those under isothermal conditions at the same temperature. When the cooling rate increased, the average width, volume fraction, and

critical precipitation temperatures of lamellar α phase decreased; additionally, the morphology of α phase gradually changed from lamellar to acicular.

(2) Mo diffusion controlled the precipitation of lamellar α phase of IMI834 titanium alloy under heat treatment. When the cooling rate increased, there was not enough time for the solutes Mo and Nb to exit the parent β phase and for the solute Al to be absorbed into the parent β phase, and thus the diffusion of the solutes Al, Mo, and Nb in α and β phases became slow. Furthermore, there was not enough time for the parent β phase to transform into α phase. This limited diffusion was the essential reason for the decrease in the volume fraction and critical precipitation temperatures of lamellar α phase.

(3) The equilibrium volume fraction and solute concentration of lamellar α phase were state functions of the transformation temperature under isothermal conditions, whereas the volume fraction and solute concentration of lamellar α phase were path functions that depended on the temperature and cooling rate under non-isothermal conditions.

(4) When the cooling rate fell into the scope of typical air and furnace cooling rates, as the cooling rate increased, the average width and volume fraction of lamellar α phase decreased from 7 to 2 μm and 85% to 37%, respectively. If the required average width of lamellar α phase was much larger than 7 μm, holding temperature at higher temperature for longer time and subsequent furnace cooling were possibly better choices.

Acknowledgments

The authors would like to gratefully acknowledge financial supports from the National Natural Science Foundation of China (No. 51675433), and the Natural Science Foundation for Distinguished Young Scholars of Shaanxi Province, China (No. 2019JC-09). The Analytical & Testing Center of Northwestern Polytechnical University is also acknowledged for the experimental support of this work.

References

[1] GHAVAM M H, MORAKABATI M, ABBASI S M, BADRI H. Flow behavior modeling of IMI834 titanium alloy during hot tensile deformation [J]. Transactions of Nonferrous Metals Society of China, 2015, 25: 748−758.

[2] WU Chuan, YANG He, LI Hong-wei. Modeling of discontinuous dynamic recrystallization of a near-α titanium alloy IMI834 during isothermal hot compression by combining a cellular automaton model with a crystal plasticity finite element method [J]. Computational Materials Science, 2013, 79: 944−959.

[3] JAYAPRAKASH M, KOMATSU D, OKAZAKI M, MIYASHITA Y, OTSUKA Y, MUTOH Y. High temperature fretting fatigue behavior of IMI 834 titanium alloy [J]. Transactions of the Indian Institute of Metals, 2016, 69: 439−444.

[4] WANG S Q, LI W Y, ZHOU Y, LI X, CHEN D L. Tensile and fatigue behavior of electron beam welded dissimilar joints of Ti−6Al−4V and IMI834 titanium alloys [J]. Materials Science and Engineering A, 2016, 649: 146−152.

[5] LEYENS C, PETERS M. Titanium and titanium alloys: Fundamentals and applications [M]. Chichester: Wiley-VCH, 2003.

[6] BALASUNDAR I, RAGHU T, KASHYAP B P. Correlation between microstructural features and tensile properties in near-α titanium alloy IMI834 processed in the α+β regime [J]. Materials Performance and Characterization, 2019, 8: 932−945.

[7] ZHOU Can-xu, LIU Bin, LIU Yong, QIU Cong-zhang, LI Hui-zhong, HE Yue-hui. Effect of carbon on high temperature compressive and creep properties of β-stabilized TiAl alloy [J]. Transactions of Nonferrous Metals Society of China, 2017, 27: 2400−2405.

[8] TAN Chang-sheng, SUN Qiao-yan, ZHANG Guo-jun, ZHAO Yong-qing. Remarkable increase in high-cycle fatigue resistance in a titanium alloy with a fully lamellar microstructure [J]. International Journal of Fatigue, 2020, 138: 105724.

[9] CHEN Kui-wai, PAN Su-ping, LIU Hui-qun, JIANG Yong. Effect of α phase morphology on fatigue crack growth behavior of Ti−5Al−5Mo−5V−1Cr−1Fe alloy [J]. Transactions of Nonferrous Metals Society of China, 2020, 30: 2459−2471.

[10] SEMIATIN S L, KNISLEY S L, FAGIN P N, BARKER D R, ZHANG F. Microstructure evolution during alpha-beta heat treatment of Ti−6Al−4V [J]. Metallurgical and Materials Transactions A, 2003, 34: 2377−2386.

[11] KATZAROV I, MALINOV S, SHA W. Finite element modeling of the morphology of β to α phase transformation in Ti−6Al−4V alloy [J]. Metallurgical and Materials Transactions A, 2002, 33: 1027−1040.

[12] GEY N, BOCHER P, UTA E, GERMAIN L, HUMBERT M. Texture and microtexture variations in a near-α titanium forged disk of bimodal microstructure [J]. Acta Materialia, 2012, 60: 2647−2655.

[13] NING Yong-quan, YAO Ze-kun, GUO Hong-zhen, FU Ming-wang. Structural-gradient-materials produced by gradient temperature heat treatment for dual-property turbine disc [J]. Journal of Alloys and Compounds, 2013, 557: 27−33.

[14] GAMSJÄGER E, LIU Y, RESTER M, PUSCHNIG P, DRAXL C, CLEMENS H, DEHM G, FISCHER F D. Diffusive and massive phase transformations in Ti−Al−Nb alloys—Modelling and experiments [J]. Intermetallics, 2013, 38: 126−138.

[15] SONG K J, WEI Y H, DONG Z B, ZHAN X H, ZHENG W J, FANG K. Numerical simulation of β to α phase transformation in heat affected zone during welding of TA15 alloy [J]. Computational Materials Science, 2013, 72: 93−100.
[16] LIU Xue-yan, LI Hong-wei, ZHAN Mei. Formation mechanism of lamellar alpha in titanium through accurate simulation [J]. Journal of Alloys and Compounds, 2019, 811: 152085.
[17] FUJII H, SUZUKI H G. Effect of cooling rates on microstructures of β treated α+β titanium alloys [J]. Tetsu-to-Hagane, 2010, 77: 1481−1488.
[18] TIAN X J, ZHANG S Q, WANG H M. The influences of anneal temperature and cooling rate on microstructure and tensile properties of laser deposited Ti−4Al−1.5Mn titanium alloy [J]. Journal of Alloys and Compounds, 2014, 608: 95−101.
[19] QIANG Feng-ming, KOU Hong-chao, TANG Bin, SONG Lin, LI Jin-shan. Effect of cooling rate on microstructure evolution of Ti−45Al−8.5Nb−0.2W−0.2B−0.02Y alloy during multi-step heat treatment [J]. Materials Characterization, 2018, 145: 210−217.
[20] SEMIATIN S L, LEHNER T M, MILLER J D, DOHERTY R D, FURRER D U. Alpha/beta heat treatment of a titanium alloy with a nonuniform microstructure [J]. Metallurgical and Materials Transactions (Part A), 2007, 38: 910−921.
[21] MENG M, YANG H, FAN X G, YAN S L, ZHAO A M, ZHU S. On the modeling of diffusion-controlled growth of primary alpha in heat treatment of two-phase Ti-alloys [J]. Journal of Alloys and Compounds, 2017, 691: 67−80.
[22] SONG K J, WEI Y H, DONG Z B, WANG X Y, ZHENG W J, FANG K. Cellular automaton modeling of diffusion, mixed and interface controlled phase transformation [J]. Journal of Phase Equilibria and Diffusion, 2015, 36: 136−148.
[23] SENKOV O N, VALENCIA J J, SENKOVA S V, CAVUSOGLU M, FROES F H. Effect of cooling rate on microstructure of Ti−6Al−4V forging [J]. Materials Science and Technology, 2013, 18: 1471−1478.
[24] BEHERA M, MYTHILI R, RAJU S, SAROJA S. Effect of cooling rate on mechanism of $\beta\rightarrow\alpha$ phase transformation on continuous cooling in Ti−5Ta−1.8Nb alloy [J]. Journal of Alloys and Compounds, 2013, 553: 59−68.
[25] CHANG Hui, GAUTIER E, BRUNESEAUX F, ZHOU Lian. $\beta\rightarrow\alpha$+β isothermal phase transformation kinetics in Ti-*B*19 metastable titanium alloy [J]. Rare Metal Materials and Engineering, 2006, 35: 1696−1699.
[26] FAN X G, YANG H. Internal-state-variable based self-consistent constitutive modeling for hot working of two-phase titanium alloys coupling microstructure evolution [J]. International Journal of Plasticity, 2011, 27: 1833−1852.
[27] LIU Geng, LI Jun, ZHANG Shen-gen, WANG Jian, MENG Qing-ge. Dilatometric study on the recrystallization and austenization behavior of cold-rolled steel with different heating rates [J]. Journal of Alloys and Compounds, 2016, 666: 309−316.
[28] KHERROUBA N, BOUABDALLAH M, BADJI R, CARRON D, AMIR M. Beta to alpha transformation kinetics and microstructure of Ti−6Al−4V alloy during continuous cooling [J]. Materials Chemistry and Physics, 2016, 181: 462−469.
[29] LI Guo-chao, CHENG Xu, TIAN Xiang-jun. Effects of annealing temperature and cooling rate on microstructures of a novel titanium alloy Ti−6Al−2V−1.5Mo−0.5Zr−0.3Si manufactured by laser additive manufacturing [J]. Journal of Iron and Steel Research International, 2018, 25: 442−452.

IMI834 钛合金等温和非等温热处理过程中片层 α 相析出行为的定量表征

刘雪艳[1,2]，李宏伟[1,2]，詹 梅[1,2]，张洪瑞[1,2]

1. 西北工业大学 材料科学与工程学院 凝固技术国家重点实验室，西安 710072；
2. 西北工业大学 陕西省高性能精确成形技术与装备重点实验室，西安 710072

摘 要：为了揭示冷却速度对片层 α 相析出的影响机制，采用试验分析方法对 IMI834 钛合金在等温和非等温热处理过程中片层 α 相的析出行为进行定量表征。通过热膨胀试验获得不同冷却速度下片层 α 相的临界析出温度。基于金相显微镜和电子探针分析以及数据拟合方法，建立片层 α 相的平均宽度、体积分数以及 α 和 β 相内的溶质浓度随温度和冷却速度的定量演化模型。两种条件下的片层 α 相析出行为对比发现：非等温冷却过程中片层 α 相的平均宽度和体积分数均小于同温度下等温相变过程中片层 α 相的平均宽度和体积分数。随着冷却速度的增加，片层 α 相的宽度和体积分数显著减小，临界析出温度降低。发生上述现象的原因是溶质元素 Al、Mo 和 Nb 的扩散速度随冷却速度增加而减小。

关键词：热处理；片层 α 相；析出；形貌演化；临界析出温度；体积分数模型；溶质浓度演化模型

(Edited by Wei-ping CHEN)